

HIERAMP: Coarse-to-Fine Autoregressive Amplification for Generative Dataset Distillation

Lin Zhao^{1*} Xinru Jiang^{1*} Xi Xiao² Qihui Fan¹ Lei Lu¹
Yanzhi Wang¹ Xue Lin¹ Octavia Camps¹ Pu Zhao^{1†} Jianyang Gu^{3†}
¹ Northeastern University ² University of Alabama at Birmingham ³ The Ohio State University

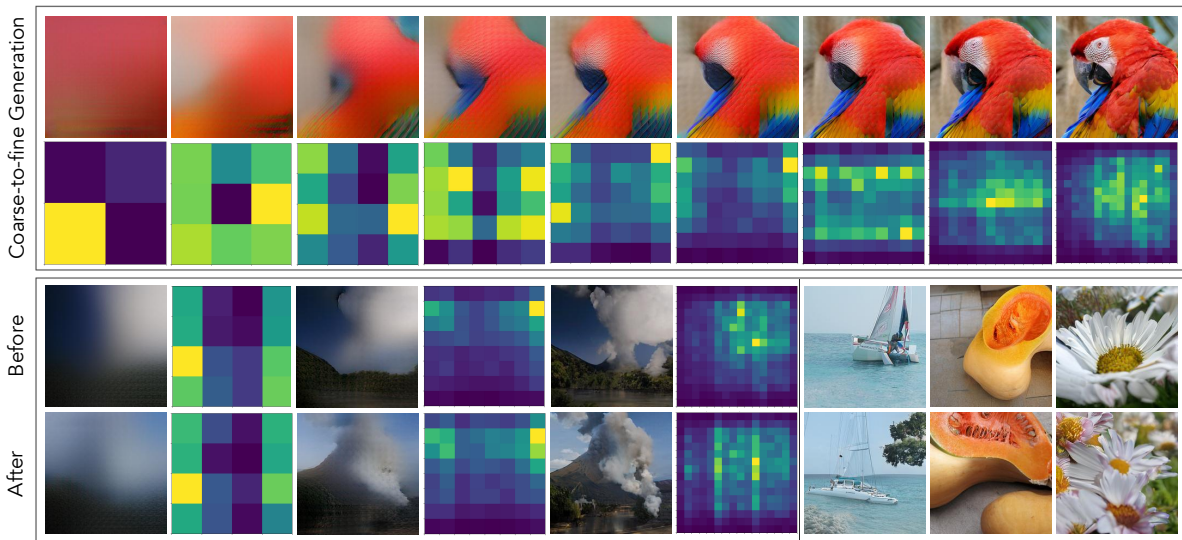


Figure 1. **Top:** The visual autoregressive model constructs coarse scene structure and gradually complements details from coarse to fine scales. The class token highlights regions that express object-related semantics (the second row). **Bottom:** HIERAMP identifies important semantic regions and refines the hierarchical structure and details in an autoregressive manner. The images after amplification demonstrate more diverse components and richer class-related details.

Abstract

Dataset distillation often prioritizes global semantic proximity when creating small surrogate datasets for original large-scale ones. However, object semantics are inherently hierarchical. For example, the position and appearance of a bird’s eyes are constrained by the outline of its head. Global proximity alone fails to capture how object-relevant structures at different levels support recognition. In this work, we investigate the contributions of hierarchical semantics to effective distilled data. We leverage the vision autoregressive (VAR) model whose coarse-to-fine generation mirrors this hierarchy and propose HIERAMP to amplify semantics at different levels. At each VAR scale, we inject class tokens that dynamically identify salient regions and use their in-

duced maps to guide amplification at that scale. This adds only marginal inference cost while steering synthesis toward discriminative parts and structures. Empirically, we find that semantic amplification leads to more diverse token choices in constructing coarse-scale object layouts. Conversely, at fine scales, the amplification concentrates token usage, increasing focus on object-related details. Across popular dataset distillation benchmarks, HIERAMP consistently improves validation performance without explicitly optimizing global proximity, demonstrating the importance of semantic amplification for effective dataset distillation.

🔗 <https://github.com/Oshikaka/HIERAMP>

1. Introduction

Dataset distillation aims to synthesize a small surrogate dataset from a large training corpus while preserving down-

*Equal contribution; † Corresponding author

stream performance. Most previous efforts optimize global distributional proximity, where features or training dynamics between synthetic and real data are matched [3, 5, 10, 26]. While reproducing the overall distribution, the distillation process does not directly reflect key factors that influence downstream performance. A distilled set may look close to the original set, but underrepresent the discriminative semantics that models use to separate classes.

In this work, we investigate dataset distillation from the perspective of object semantics, as a complement to distributional proximity. The semantics of a specific object in an image are inherently hierarchical [27, 30, 57]. As shown in 1, the global layout governs the coarse-level spatial organization and object placement. At a finer granularity, the semantics of individual parts constrain the associated textures and details. Vision autoregressive (VAR) models naturally reflect this characteristic by synthesizing images in a coarse-to-fine manner [31, 42]. Early scales generate the overall structure, while deeper scales focus more on subtle details. Our method exploits this alignment and explores the effect of object-related semantics at different scales.

Based on this, we propose HIERAMP to amplify the generation process in an autoregressive fashion. Concretely, we inject learnable class tokens into each scale of the VAR model and optimize them with a classification objective [49]. During generation, the class token of scale ℓ aggregates context and produces a soft importance map over spatial tokens. The map highlights regions with object-related semantics expressed at that scale. Therefore, we amplify attention toward tokens with higher importance scores during autoregressive decoding. Compared with adopting external segmentation tools [25], the design adds only a marginal inference cost and avoids heavy guidance at test time. More importantly, it allows for more fine-grained salient identification across different generation scales. This framework enables the analysis of semantics at different hierarchical levels. We examine the change of token-distribution diagnostics (*e.g.*, entropy and token coverage) before and after amplifying the attention along the VAR scales. Empirically, we find that the amplification leads to distinct effects at different generation scales. For coarse scales, the token distribution becomes more uniform and diverse. Oppositely, the amplification at fine scales concentrates the token usage. By comparing the validation performance, we find that amplifying coarse scales leads to the most significant accuracy improvement. Qualitatively, we show that while the coarse scales do not directly contribute to object-specific details, they set the overall structure and largely influence the semantic richness of later scales.

Extensive experiments are conducted across popular dataset distillation benchmarks, where HIERAMP achieves state-of-the-art validation accuracy. HIERAMP uncovers the relationship between hierarchical semantics and down-

stream model training, which enhances the explainability of dataset distillation. Through this work, we call for more attention toward understanding the underlying mechanisms that support effective and trustworthy dataset distillation.

2. Related Works

2.1. Dataset Distillation

Dataset Distillation (DD) [47] compresses a large training set into a small synthetic set that preserves training performance. Prior works formulate dataset distillation as a bi-level optimization problem [3, 52], mainly via gradient matching [19, 21, 43, 50, 52] or trajectory matching [3, 5, 9, 10]. However, these methods are computationally expensive and difficult to scale to high-resolution images and large datasets, with limited cross-architecture generalization. To address this, distribution matching [7, 51, 53] aligns feature statistics in embedding spaces, shifting from explicit optimization to statistical alignment. Building on this, recent efficient distillation methods [5, 19, 36, 40] further improve scalability and performance. However, images produced by these approaches often lack visual fidelity and appear perceptually unrealistic, resembling feature abstractions rather than natural images.

The above limitation motivates the adoption of generative models that prioritize visual realism and fidelity beyond purely optimization-driven objectives. Early GAN-based methods [33, 46, 57] produce more representative samples. However, they exhibit limited data diversity, which hinders effective distillation. More recently, Diffusion models [13, 14, 38, 45, 55] have emerged as the state-of-the-art approach, providing more higher quality, diverse samples that better preserve the characteristics of the original dataset.

2.2. Generative Model

Generative modeling aims to learn data distributions for realistic synthesis [11]. GANs [12] achieve high fidelity but often suffer from mode collapse and unstable training at high resolutions [1]. To improve stability and sample diversity, diffusion models [17, 37] are introduced, producing high-quality and diverse results across domains [8, 54, 56]. However, their long denoising chains incur substantial computational cost [4]. In contrast, Visual Autoregressive (VAR) models [42] introduce a coarse-to-fine hierarchy for scale-aware control, achieving competitive quality with fewer sampling steps and providing a strong generative backbone.

3. Method

3.1. Preliminary

Rather than predicting the next token as in other autoregressive generators [22, 24, 39], VAR [42] predicts the next

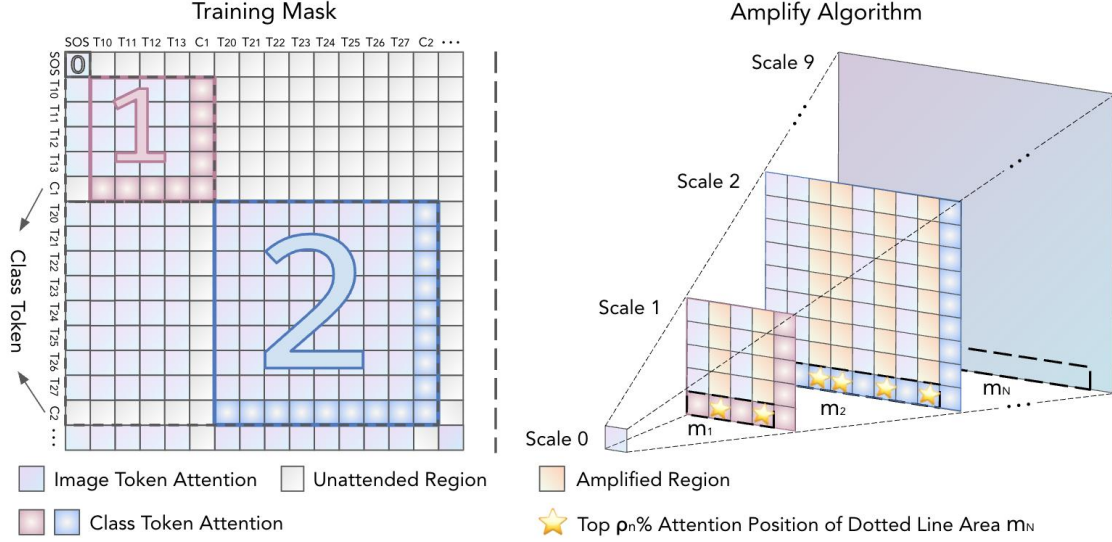


Figure 2. **Overview of the HIERAMP framework.** **Left:** Scale-Restricted Class Token Attention Mask. The class token attends only to image tokens from the corresponding scale, with grey regions indicating blocked attention, producing a scale-specific semantic summary. **Right:** Multi-Scale Semantic Feature Amplification. The Amplify Algorithm selects the top attention positions from the class-token map at each scale and amplifies them via a positive logit bias, guiding the model to focus on semantically important features during decoding.

scale over the entire token map. Since the model operates in a discrete token space, VAR employs a VQ-VAE [44] to bridge token features and images via codebook dequantization and decoding. When predicting the feature of current scale r_n , VAR uses the ground-truth feature (r_1, \dots, r_{n-1}) . During training, it minimizes the cross-entropy loss over all scales with teacher forcing as follows:

$$P = \prod_{n=1}^N p_{\theta}(r_n | r_1, \dots, r_{n-1}), \quad (1)$$

where P is the predicted feature of all scales, and p_{θ} indicates the VAR model. For the attention in transformer blocks, it adopts a scale-based masking to ensure that the tokens at scale n can only attend to earlier scales.

During inference, the model samples one scale at a time. The N scale generation can be expressed as:

$$\begin{aligned} r_1 &\sim p_{\theta}(r_1 | s), \\ r_2 &\sim p_{\theta}(r_2 | r_1), \\ &\dots \\ r_N &\sim p_{\theta}(r_N | r_1, \dots, r_{N-1}), \end{aligned} \quad (2)$$

where s is the initial class embedding. Notably, after generating the n^{th} scale, r_n is incorporated via residual addition with the upsampling feature of the $(n-1)^{\text{th}}$ scale, yielding the updating for the $(n+1)^{\text{th}}$ scale:

$$r_n = r_n + \mathcal{U}_{(n-1) \rightarrow n}(r_{n-1}), \quad (3)$$

where $\mathcal{U}_{a \rightarrow b}(\cdot)$ denotes the upsampling operator that maps features from scale a to scale b .

Intuition. VAR learns “what remains” at each finer scale and composes an image by successively adding those coarse-level layout first, then mid-level structure, and finally fine-level details.

3.2. Motivation

Current dataset distillation methods mainly operate on images monolithically, which directly match the original data distribution in pixel space [3] or latent space [38, 55]. There are two main drawbacks for these methods: (i) The feature mapping between surrogate dataset and full dataset is typically performed in a low-level structural feature space, with limited semantic understanding. (ii) All features are modeled in a single latent space, without accounting for the hierarchical nature of image information [23, 57]. This motivates us to analyze the problem from a coarse-to-fine semantic generation perspective, to identify hierarchical designs that better benefit the dataset distillation task. Consequently, the coarse-to-fine nature of VAR is tightly aligned with our objective of modeling semantics across scales.

3.3. Semantic-guided Attention Analysis

VAR is a generative model based on transformer blocks, in which self-attention provides a natural probe into how information flows during generation. Therefore, we analyze the attention features from a semantic perspective to understand what each scale encodes and how to optimize the synthesis for dataset distillation.

We begin by extracting semantic patterns from attention maps as the basis for our analysis. To achieve this, we in-

roduce learnable class tokens following DINO [2, 28]. As VAR performs residual refinement across multiple scales, the regions of focus vary by scale. Accordingly, we introduce a learnable class token at each scale to capture the semantic information. As shown in Fig. 2-left, at scale n , the class token is constrained by a scale-restricted attention mask only attend to tokens from the same scale, yielding a scale-specific semantic summary. Notably, while VAR allows regular tokens at scale n to attend to tokens from earlier scales ($1:n-1$), the class token is explicitly masked to ignore such cross-scale connections and focus exclusively on the current scale.

The attention map at scale n is denoted by $\mathbf{X}_n \in \mathbb{R}^{L_q^n \times L_k^n}$, and $[c]_n \in \mathbb{R}^d$ denotes a learnable class token. We append $[c]_n$ to obtain $\tilde{\mathbf{X}}_n = [\mathbf{X}_n, [c]_n]$. For multi-head attention with H heads, the query $\mathbf{Q}_n^{(h)}$, key $\mathbf{K}_n^{(h)}$ and value $\mathbf{V}_n^{(h)}$ for head h at scale n are computed as:

$$\mathbf{Q}_n^{(h)} = \tilde{\mathbf{X}}_n \mathbf{W}_Q^{(n)}, \quad \mathbf{K}_n^{(h)} = \tilde{\mathbf{X}}_n \mathbf{W}_K^{(n)}, \quad \mathbf{V}_n^{(h)} = \tilde{\mathbf{X}}_n \mathbf{W}_V^{(n)}, \quad (4)$$

where $\mathbf{W}_Q^{(n)}$, $\mathbf{W}_K^{(n)}$ and $\mathbf{W}_V^{(n)}$ are learnable projection matrices. Based on this, the attention map between class-token query and same-scale keys for head h can be expressed as:

$$\alpha_{n,\text{cls}}^{(h)} = \text{softmax}\left(\frac{\mathbf{Q}_n^{(h)}[:, -1] (\mathbf{K}_n^{(h)})^\top}{\sqrt{d_h}} + \mathbf{m}_{n,\text{cls}}^{(h)}\right), \quad (5)$$

where $\mathbf{m}_{n,\text{cls}}^{(h)} \in \{0, -\infty\}^{1 \times (1+L_k)}$ is zero on positions from scale n and $-\infty$ on all other positions. Given the class-token attention map $\alpha_{n,\text{cls}}^{(h)}$, we form the class token embedding \mathbf{c}_n^e , and apply a lightweight classifier $p_n(\cdot)$ to train the $[c]_n$:

$$\mathcal{L}_{\text{cls}} = \frac{1}{N} \sum_{n=1}^N \left(-\log p_n(\mathbf{c}_n^e)\right). \quad (6)$$

By assigning a unique class token to each scale, we explicitly learn the semantic information at every scale. We use $\alpha_{n,\text{cls}}^{(h)}$ as a semantic saliency map for scale n , aggregated over heads:

$$\mathbf{m}_n = \frac{1}{H} \sum_{h=1}^H \alpha_{n,\text{cls}}^{(h)} \in \mathbb{R}^{1 \times L_k}, \quad (7)$$

$$\mathbf{M}_n = \text{R}_{h_n \times w_n}(\mathbf{m}_n) \in \mathbb{R}^{h_n \times w_n},$$

where $\mathbf{m}_n \in \mathbb{R}^{1 \times L_k}$ denotes the class-token attention map aggregated over heads. R means that reshape \mathbf{m}_n to $\mathbf{M}_n \in \mathbb{R}^{h_n \times w_n}$, which aligns with the $h_n \times w_n$ token grid of the image height and weight at scale n , with $h_n w_n = L_k$. Fig. 1 visualizes \mathbf{M}_n at different scales. The highlighted areas indicate that $[c]_n$ successfully captures semantically important regions.

3.4. Coarse-to-fine Autoregressive Amplification

As shown in Fig. 2-right, we leverage the semantic class-token attention to guide autoregressive decoding from coarse to fine scales. Our model contains ten hierarchical scales indexed by $n \in \{0, \dots, 9\}$. Since scale 0 contains only a single patch (one token), we exclude it from amplification and operate on scales $n \in \{1, \dots, 9\}$. We group this into three stages: **Coarse** (1–3), **Mid** (4–6), and **Fine** (7–9), with **Full** referring to all scales 1–9. Since the high-magnitude entries of \mathbf{m}_n correspond to locations most attended by the class token $[c]_n$, we select a set of salient positions \mathcal{S}_n from \mathbf{m}_n by keeping the top $\rho_n\%$ entries:

$$\mathcal{S}_n = \text{Top-}\rho_n(\mathbf{m}_n). \quad (8)$$

Thus a binary indicator $\mathbf{a}_n \in \{0, 1\}^{L_k^n}$ on \mathbf{m}_n can be obtained according to \mathcal{S}_n :

$$(\mathbf{a}_n)_j = \begin{cases} 1, & \text{if } j \in \mathcal{S}_n, \\ 0, & \text{otherwise,} \end{cases} \quad j = 1, \dots, L_k^n. \quad (9)$$

Our goal is to steer attention toward semantically relevant regions—namely the positions j with $(\mathbf{a}_n)_j = 1$.

To make all queries at scale n preferentially attend to these salient keys, we add positive logit bias to the corresponding key columns for every head h :

$$\mathbf{L}_n^{(h)} = \frac{\mathbf{Q}_n^{(h)} (\mathbf{K}_n^{(h)})^\top}{\sqrt{d_h}} + \mathbf{p}_n^{(h)}, \quad (10)$$

$$\tilde{\mathbf{L}}_n^{(h)} = \mathbf{L}_n^{(h)} + \beta_n \mathbf{1}_{L_k^n+1} \mathbf{a}_n^\top.$$

where $\mathbf{p}_n^{(h)}$ denotes the original mask, $\mathbf{1}_{L_k^n+1}$ is an all-ones column vector matching the number of queries at the scale (including the class token), and $\beta_n > 0$ controls the amplification strength. The modified attention then becomes $\tilde{\alpha}_n^{(h)} = \text{softmax}(\tilde{\mathbf{L}}_n^{(h)})$, which increases the probability mass on semantically meaningful regions for every token at scale n . We apply this procedure from coarse to fine, using a stage-aware schedule $\rho_{1:3}, \rho_{4:6}, \rho_{7:9}$, so early scales emphasize global object regions while later scales refine fine textures. This coarse-to-fine reinforcement aligns the attention hierarchy with semantic structure and improves semantic consistency and details across generation pipeline.

4. Experiments

4.1. Experimental Settings

Datasets. We evaluate the practical applicability of our method on both large-scale and small-scale datasets. Our primary benchmark is ImageNet-1K (224 × 224) [6], which contains 1,000 classes and approximately one million images. To assess performance under limited data conditions,

Dataset	IPC	ResNet-18					ResNet-101				
		Minimax	D ³ HR	RDED	CaO ₂	Ours	Minimax	D ³ HR	RDED	CaO ₂	Ours
CIFAR-10	10	–	41.3 ± 0.1	37.1 ± 0.3	39.0 ± 1.5	44.3 ± 0.6	–	35.8 ± 0.6	33.7 ± 0.3	–	64.3 ± 0.9
	50	–	70.8 ± 0.5	62.1 ± 0.1	–	72.0 ± 0.1	–	63.9 ± 0.4	51.6 ± 0.4	–	64.3 ± 0.9
CIFAR-100	10	–	49.4 ± 0.2	42.6 ± 0.2	–	52.0 ± 0.1	–	46.0 ± 0.5	41.1 ± 0.2	–	49.7 ± 0.2
	50	–	65.7 ± 0.3	62.6 ± 0.1	–	66.5 ± 0.2	–	66.6 ± 0.2	63.4 ± 0.3	–	66.1 ± 0.2
ImageNet-Woof	1	19.9 ± 0.2	–	20.8 ± 1.2	21.1 ± 0.6	20.9 ± 0.8	17.7 ± 0.9	–	19.6 ± 1.8	21.2 ± 1.7	20.3 ± 1.4
	10	40.1 ± 1.0	39.6 ± 1.0	38.5 ± 2.1	45.6 ± 1.4	45.8 ± 1.6	34.2 ± 1.7	–	31.3 ± 1.3	36.5 ± 1.4	39.0 ± 1.4
	50	67.0 ± 1.8	57.6 ± 0.4	68.5 ± 0.7	68.9 ± 1.1	70.0 ± 0.8	62.7 ± 1.6	–	59.1 ± 0.7	63.1 ± 1.3	66.2 ± 1.2
ImageNet-100	1	7.3 ± 0.1	–	8.1 ± 0.3	8.8 ± 0.4	8.9 ± 0.3	5.4 ± 0.6	–	6.1 ± 0.8	6.6 ± 0.4	6.24 ± 0.4
	10	32.0 ± 1.0	–	36.0 ± 0.3	36.6 ± 0.2	36.7 ± 0.3	29.2 ± 1.0	–	33.9 ± 0.1	34.5 ± 0.4	35.1 ± 0.2
	50	63.9 ± 0.1	–	61.6 ± 0.1	68.0 ± 0.5	68.1 ± 0.2	67.4 ± 0.6	–	66.0 ± 0.6	70.8 ± 0.2	66.1 ± 0.4
ImageNet-1K	1	5.9 ± 0.2	–	6.6 ± 0.2	7.1 ± 0.1	7.7 ± 0.1	4.0 ± 0.5	–	5.9 ± 0.4	6.0 ± 0.4	6.8 ± 0.4
	10	44.3 ± 0.5	44.3 ± 0.3	42.0 ± 0.1	46.1 ± 0.2	47.6 ± 0.1	46.9 ± 1.3	52.1 ± 0.4	48.3 ± 1.0	52.2 ± 1.1	50.8 ± 0.4
	50	58.6 ± 0.3	59.4 ± 0.1	56.5 ± 0.1	60.0 ± 0.0	60.8 ± 0.5	65.5 ± 0.1	66.1 ± 0.1	61.2 ± 0.4	66.2 ± 0.1	66.4 ± 0.3
	100	–	62.5 ± 0.0	–	–	62.7 ± 0.3	–	68.1 ± 0.0	–	–	68.5 ± 0.3

Table 1. **Top-1 accuracy comparison with four SOTA methods.** As in RDED [40], all methods adopt ResNet-18 as the teacher and are trained on both ResNet-18 and ResNet-101. ‘–’ denotes missing results in the original paper.

we also use CIFAR-10 and CIFAR-100 (32×32) [20], ImageWoof [18], a subset of 10 dog breeds, and ImageNet-100 [32], which includes 100 randomly selected classes from ImageNet-1K. To explore higher compression ratios while maintaining generalizability, we experiment with three images-per-class (IPC) settings: 1, 10, and 50, across all datasets, and include an IPC of 100 for ImageNet-1K.

Network Architectures. Following previous works [40, 55], we evaluate our method on a variety of neural network architectures to confirm its performance. The experiments include ResNet-18 & ResNet-101 [15], MobileNet-V2 [34], and EfficientNet-B0 [41]. All experiments are conducted three times to ensure fair and reliable comparisons with other methods.

Baselines. We compare HIERAMP against four state-of-the-art methods: Minimax [13], which formulates distillation as a minimax optimization to enhance generalization by utilizing diffusion models; D³HR [55], a DDIM inversion approach that improves high-resolution synthesis by distribution matching; RDED [40], which preserves visual realism by selecting and cropping informative patches directly from real images; and CaO₂ [45], a diffusion-driven method that combines probabilistic sample selection with latent-code refinement to enhance conditional likelihood.

Implementation Details. We adopt the pre-trained Visual Autoregressive Model (VAR) [42] with a depth of 16 and the resolution of 256×256 , originally trained on ImageNet. The model is then fine-tuned for 5 epochs with a class token for semantic-guided attention. All experiments are conducted on NVIDIA RTX A6000 GPUs.

4.2. Comparison with State-of-the-art Methods

We evaluate the effectiveness of HIERAMP against four state-of-the-art dataset distillation approaches: Minimax [13], D³HR [55], RDED [40], and CaO₂ [45]. Following

the RDED evaluation protocol, all methods use ResNet-18 as the teacher and are separately trained and evaluated on ResNet-18 and ResNet-101. Missing results (‘–’) indicate entries not reported in the original papers. As shown in Table 1, HIERAMP achieves the highest performance across most datasets and IPC settings.

Small-scale Datasets. For CIFAR-10, our method reaches 44.3% and 72.0% on ResNet-18 at IPC= 10 and 50, respectively, outperforming the previous best method D³HR. On CIFAR-100, HIERAMP also achieves the highest accuracy at IPC= 10 and remains competitive with the strongest baselines at IPC= 50. On ImageNet-Woof, for IPC=10, it outperforms RDED by 6.2% on ResNet-18 and 7.7% on ResNet-101. Our method surpasses all other baselines at both IPC=10 and IPC=50, reaching 70.0% at IPC=50.

Mid-scale Datasets. When scaling to ImageNet-100, it outperforms RDED and CaO₂ across most IPCs, achieving the highest accuracy of 68.14% on ResNet-18 at IPC=50.

Large-scale Datasets. On the large-scale ImageNet-1K, it demonstrates a clear advantage. At IPC=1, it exceeds Minimax by 1.8% and RDED by 1.1% on ResNet-18. At IPC=10, it achieves 47.6% on ResNet-18, outperforming the second-best method, CaO₂, by 1.5%, while maintaining competitive performance on ResNet-101. At high IPCs (50 and 100), HIERAMP consistently surpasses all baselines, highlighting its robust scalability to larger datasets.

Besides, we report Frechet Inception Distance (FID) [16] and computational efficiency comparisons with other methods, which can be seen in Appendix C and E.

4.3. Cross-architecture Generalization

We further evaluate the generalization ability of our method across different network architectures. Table 2 reports the Top-1 accuracy on ImageNet-1K (IPC=10) when distilled datasets generated by a teacher network are used to

Student\Teacher		ResNet-18	MobileNet-V2	EfficientNet-B0
ResNet-18	RDED	42.3 ± 0.6	40.4 ± 0.1	36.6 ± 0.1
	D ³ HR	44.3 ± 0.3	42.3 ± 0.7	38.3 ± 0.2
	Ours	44.6 ± 0.5	42.9 ± 0.3	38.7 ± 0.1
MobileNet-V2	RDED	34.4 ± 0.2	33.8 ± 0.6	28.7 ± 0.2
	D ³ HR	43.4 ± 0.3	46.4 ± 0.2	37.8 ± 0.4
	Ours	46.2 ± 0.1	45.8 ± 0.3	38.0 ± 0.2
EfficientNet-B0	RDED	22.7 ± 0.1	21.6 ± 0.2	23.5 ± 0.3
	D ³ HR	25.7 ± 0.4	24.8 ± 0.4	28.1 ± 0.1
	Ours	25.9 ± 0.3	25.1 ± 0.2	28.7 ± 0.4

Table 2. **Cross-architecture performance on ImageNet-1K, IPC=10.**

Amp. - $\rho_n\%$	Coarse	Mid	Fine	Full
0 - 0%	45.6 ± 0.3			
5 - 30%	46.7 ± 0.2	46.3 ± 0.1	46.6 ± 0.3	46.9 ± 0.2
5 - 70%	47.0 ± 0.3	46.4 ± 0.2	46.2 ± 0.3	46.6 ± 0.2
3 - 50%	46.8 ± 0.2	46.7 ± 0.3	46.5 ± 0.1	47.1 ± 0.1
7 - 50%	47.3 ± 0.2	47.4 ± 0.3	46.3 ± 0.2	47.2 ± 0.3
5 - 50%	47.6 ± 0.3	46.9 ± 0.1	46.5 ± 0.2	47.6 ± 0.1

Table 3. **Effect of amplification combination across different stages on ImageNet-1K, IPC=10.** Amp. indicates the amplification number, while $\rho_n\%$ refers to the top $\rho_n\%$ of the m_N regions selected for amplification.

train various student architectures, including ResNet-18, MobileNet-V2, and EfficientNet-B0.

Compared to state-of-the-art distillation methods RDED [40] and D³HR [55], our approach consistently achieves the highest accuracy across almost all of the teacher-student pairs. Notably, when using a MobileNet-V2 teacher, our distilled dataset enables a ResNet-18 student to reach 46.2%, surpassing both RDED and D³HR by a substantial margin. These results demonstrate that HIERAMP produces realistic representative samples with strong cross-architecture generalization.

4.4. Ablation Study

Effect of Amplification Combination Across Stages. We evaluate the impact of different amplification strategies on ImageNet-1K with IPC=10. Specifically, we vary the amplification number (Amp.) and the proportion of top attention regions ($\rho_n\%$) selected for amplification at each stage (Coarse, Mid, Fine, Full). Table 3 reports the accuracy for each configuration.

Without any amplification (0 – 0%), the baseline performance is 45.6%. Introducing selective amplification consistently improves accuracy across all stages. For instance, amplifying 5 regions with 30% top attention (5 – 30%) raises the full-stage accuracy to 46.9%, while amplifying 3 regions with 50% top attention (3 – 50%) further improves it to 47.1%. Increasing the amplification number to 5 at 50%

C-M-F	0.1-5-5	5-0.1-5	5-5-0.1
Top-1 Acc. (%)	45.9 ± 0.1	46.6 ± 0.1	46.6 ± 0.3
C-M-F	0.5-5-5	5-0.5-5	5-5-0.5
Top-1 Acc. (%)	46.3 ± 0.2	46.5 ± 0.3	46.8 ± 0.3

Table 4. **Ablation on amplification strength across stages on ImageNet-1K, IPC=10.** Each row shows a different setting of Coarse-Mid-Fine (C-M-F) amplification numbers and accuracy.

top attention (5 – 50%) achieves the best overall performance, reaching 47.6% at both the Coarse and Full stages, demonstrating that moderate amplification focused on top attention regions effectively enhances model performance.

These results indicate that carefully combining amplification across hierarchical stages allows the model to better focus on semantically relevant regions, leading to consistent gains over the non-amplified baseline.

Ablation on Amplification Strength Across Stages. We investigate the effect of varying amplification strength across hierarchical stages (Coarse, Mid, Fine) on ImageNet-1K with IPC=10. Table 4 reports the Top-1 accuracy for different combinations of amplification numbers applied to the Coarse-Mid-Fine (C-M-F) stages.

From the results, we observe that the model is sensitive to the distribution of amplification across stages. When the Coarse stage receives minimal amplification (0.1) while Mid and Fine stages are heavily amplified (5), the accuracy is relatively low (45.9%). Increasing the Coarse stage amplification to moderate levels (0.5–5–5) improves performance to 46.3%, indicating that Coarse-stage attention contributes to capturing global structural information.

Moreover, balancing amplification across stages, e.g., applying higher amplification to Fine stage while maintaining moderate Coarse and Mid stages (5–5–0.5), achieves best accuracy of 46.8%. These findings suggest that distributing amplification across hierarchical stages allows model to effectively focus on both global and local object features, resulting in improved recognition performance.

5. Analysis and Insights

Building on the enhanced empirical results, we further analyze why and how attention amplification improves the distilled data. We use the same three-stage split as in the method design. Each image can be encoded into a set of discrete codebook token maps across multiple scales using a vector-quantized VAE (VQ-VAE) with a codebook size of 4096 [42]. For each token i in the codebook, we can acquire the occurrence count n_i and the normalized occurrence probability p_i of it appearing in a given dataset:

$$p_i = \frac{n_i}{\sum_j n_j}. \quad (11)$$

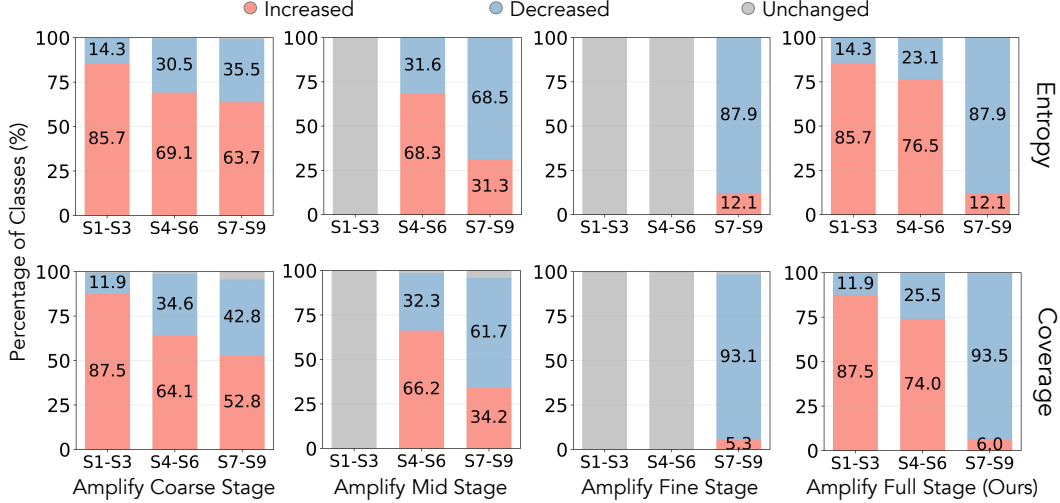


Figure 3. **Impact of attention amplification strategy on token entropy and coverage on ImageNet-1K, IPC=50.** The histogram shows the percentage of classes whose codebook token entropy and coverage increased, decreased, or remained unchanged after amplifying different stages. Amplifying attention at coarse and mid scales promotes diversity, while fine-scale amplification can concentrate attention.

Subsequently, we analyze on the dataset, class, and sample levels to illustrate the influence of attention amplification on different hierarchical stages.

5.1. Dataset-level

To study the overall token distribution across classes, we adopt two statistical measures: Entropy [35] and Coverage [48]. These metrics comprehensively quantify the uncertainty and utilization rate of the codebook token usage, respectively. More concretely, we compute these metrics from the occurrence counts of codebook tokens at each scale. The Entropy H is defined as:

$$H = - \sum_{i=1}^N p_i \log p_i. \quad (12)$$

A higher entropy indicates a more uniform and diverse token distribution. The Coverage is defined as:

$$\text{Coverage} = \frac{N_{\text{used}}}{N_{\text{total}}}, \quad (13)$$

where N_{used} is the number of unique tokens that appear at least once, and N_{total} is 4096, the entire codebook size. Higher coverage indicates broader utilization of codebook.

We measure the change in token entropy and coverage across different amplification stages. The percentage of classes with increased, decreased, and unchanged metric values after amplification is summarized in Fig. 3. Only amplifying attention in the **Coarse** stage increases both entropy and coverage for most classes, indicating enhanced token diversity and more distributed token usage. Amplifying the **Mid** stage increases the entropy of entropy and coverage for itself, yet decreases the metric for the Fine stage.

Amplification only at the **Fine** stage leads to more substantial entropy reduction, implying more focused and repetitive token activation. The **Full** stage amplification (ours) combines all the above effects, increasing entropy for the coarse and mid stages while decreasing that for the fine stage.

These changes indicate that at coarse stages, the semantics of salient regions are rich and diverse. Amplifying those semantics leads to even more different compositions of tokens. Oppositely, at the fine stage, VAR focuses on refining object-specific details. Therefore, after amplification, the token selection is more concentrated. Based on the results in Tab. 3, the amplification at the coarse stage is more effective than that at the fine stage. This result indicates that coarse-level richness has a more significant influence on the final model performance. We include the effects visualization of more amplification settings in the Supplementary Material.

5.2. Class-level

From Fig. 4, we observe that amplifying coarse stages increases the overall token diversity across patches, evidenced by more dark (e.g. purple) blocks on the heatmap. Amplification on the other two stages only has a moderate influence on per-patch token diversity. Our strategy of full amplification aligns with this trend, at coarse and mid stage the model will have more choice of codebook token, which can generate more diverse images; at fine stage, it will refine the details and textures. Although the dataset-level token usage is concentrated at fine scales, within each dataset, the diversity is preserved to maintain rich spatial structures.

We examine the effect of amplification within a specific class. For Fig. 4, amplifying the **Coarse** stages increases token diversity across patch positions, reflected by the larger

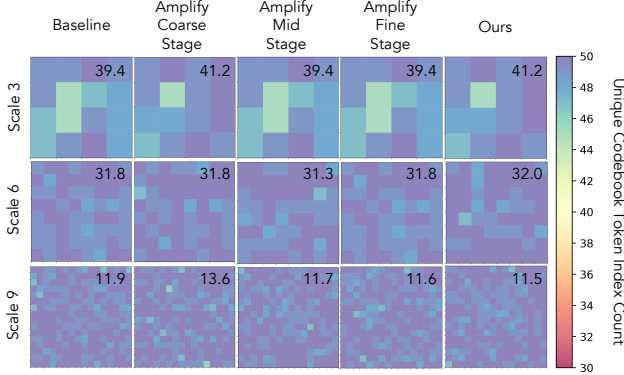


Figure 4. **Heatmap of unique codebook token occurrences across patch positions and scales on ImageNet-1K, Class 51 – Triceratops, IPC=50.** Darker patches indicate a higher number of unique tokens. The average of unique-token count for each scale is displayed in the upper-right corner of each heatmap.

number of dark (e.g., purple) cells in the heatmaps. In contrast, amplification at the **Mid** and **Fine** stages induces only moderate changes in per-patch token diversity.

This behavior is consistent with our **Full** amplification strategy. At the **Coarse** and **Mid** stages, amplification expands the set of available codebook tokens, enabling the model to produce more diverse global structures. At the **Fine** stage, the model instead focuses on refining local details and textures. Although token usage at the dataset level is more concentrated at fine scales, the per-class distributions remain diverse, preserving the spatial richness necessary for high-quality image generation.

5.3. Sample-level

We additionally visualize the amplification effects at different stages with specific samples to understand their differences and examine the amplified regions. Across all the scales, we observe that the attention of the class token is stronger after amplification, indicating that these regions become more class-related.

Coarse Stage. At the initial scales, our method primarily captures the overall structure of the object. As illustrated in Fig. 5 at Scale 3, attention is focused on the main object regions, revealing the butternut squash’s distinctive orange hue and the daisy’s white petals. After amplification, the color becomes more vivid, indicating a richer and more diverse selection of codebook tokens. This suggests that the model establishes a strong global representation of the object while maintaining token variability. While these semantics do not directly describe discriminative details, the amplification provides more possible token compositions at later stages.

Mid Stage. At intermediate scales, attention becomes more semantically refined. The model selectively emphasizes

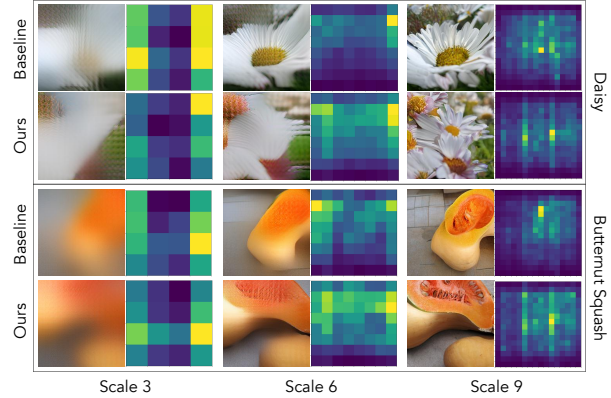


Figure 5. **Example generated images and attention heatmaps of the class token.** Our method produces richer object details and quantities, achieves stronger semantic alignment, and enhances object-background dependence.

distinctive object parts, such as the internal and surface features of the squash. Fig. 5 stage 6 shows improved alignment between attention and object semantics, demonstrating that residuals generated at this stage become more closely tied to the target objects. We also observe that combined amplifications at coarse and mid stages can generate multiple object instances, further supporting the view that the amplified semantics are object-related.

Fine Stage. At fine scales, attention spreads over semantically relevant regions in greater detail. In the squash case, attention is mainly focused on the cross-section of the squash, where finer details of texture and shadows are being added. In comparison, not as much attention is paid to the background or other squashes at the side. It also corresponds to the more concentrated token usage as suggested in Fig. 5. These refined details provide a moderate performance improvement for training classification models.

6. Conclusion

We propose HIERAMP, a hierarchical attention framework for dataset distillation that leverages the coarse-to-fine structure of VAR models. Our method injects learnable class tokens and amplifies attention at each scale to capture object-level semantics, addressing the lack of semantic guidance in existing distillation approaches. HIERAMP achieves SOTA performance on ImageNet-1K and its subsets, and provides interpretable insights into scale-specific token distributions.

Acknowledgments

This research is supported in part by grants from ONR N00014-21-1-2431, NSF OAC-211824, NSF IIS-2310254.

References

- [1] Jonas Adler and Sebastian Lunz. Banach wasserstein gan. In *Advances in neural information processing systems*, 2018. 2
- [2] Mathilde Caron, Hugo Touvron, Ishan Misra, Hervé Jégou, Julien Mairal, Piotr Bojanowski, and Armand Joulin. Emerging properties in self-supervised vision transformers. In *Proceedings of the IEEE/CVF international conference on computer vision*, pages 9650–9660, 2021. 4
- [3] George Cazenavette, Tongzhou Wang, Antonio Torralba, Alexei A Efros, and Jun-Yan Zhu. Dataset distillation by matching training trajectories. In *Proceedings of the IEEE/CVF Conference on Computer Vision and Pattern Recognition*, pages 4750–4759, 2022. 2, 3
- [4] Florinel-Alin Croitoru, Vlad Hondru, Radu Tudor Ionescu, and Mubarak Shah. Diffusion models in vision: A survey. *IEEE transactions on pattern analysis and machine intelligence*, 45(9):10850–10869, 2023. 2
- [5] Justin Cui, Ruochen Wang, Si Si, and Cho-Jui Hsieh. Scaling up dataset distillation to imagenet-1k with constant memory. In *International Conference on Machine Learning*, pages 6565–6590. PMLR, 2023. 2
- [6] Jia Deng, Wei Dong, Richard Socher, Li-Jia Li, Kai Li, and Li Fei-Fei. Imagenet: A large-scale hierarchical image database. In *2009 IEEE conference on computer vision and pattern recognition*, pages 248–255. Ieee, 2009. 4
- [7] Wenxiao Deng, Wenbin Li, Tianyu Ding, Lei Wang, Hongguang Zhang, Kuihua Huang, Jing Huo, and Yang Gao. Exploiting inter-sample and inter-feature relations in dataset distillation. In *Proceedings of the IEEE/CVF Conference on Computer Vision and Pattern Recognition*, pages 17057–17066, 2024. 2
- [8] Prafulla Dhariwal and Alexander Nichol. Diffusion models beat gans on image synthesis. In *Advances in neural information processing systems*, 2021. 2
- [9] Jiawei Du, Yidi Jiang, Vincent YF Tan, Joey Tianyi Zhou, and Haizhou Li. Minimizing the accumulated trajectory error to improve dataset distillation. In *Proceedings of the IEEE/CVF conference on computer vision and pattern recognition*, pages 3749–3758, 2023. 2
- [10] Jiawei Du, Qin Shi, and Joey Tianyi Zhou. Sequential subset matching for dataset distillation. *Advances in Neural Information Processing Systems*, 36, 2024. 2
- [11] Ian Goodfellow, Yoshua Bengio, and Aaron Courville. *Deep Learning*. MIT Press, 2016. 2
- [12] Ian J Goodfellow, Jean Pouget-Abadie, Mehdi Mirza, Bing Xu, David Warde-Farley, Sherjil Ozair, Aaron Courville, and Yoshua Bengio. Generative adversarial nets. In *Advances in neural information processing systems*, 2014. 2
- [13] Jianyang Gu, Saeed Vahidian, Vyacheslav Kungurtsev, Haonan Wang, Wei Jiang, Yang You, and Yiran Chen. Efficient Dataset Distillation via Minimax Diffusion. In *Proceedings of the IEEE/CVF Conference on Computer Vision and Pattern Recognition (CVPR)*, 2024. 2, 5, 1
- [14] Jianyang Gu, Haonan Wang, Ruoxi Jia, Saeed Vahidian, Vyacheslav Kungurtsev, Wei Jiang, and Yiran Chen. Concord: Concept-informed diffusion for dataset distillation. *arXiv preprint arXiv:2505.18358*, 2025. 2
- [15] Kaiming He, Xiangyu Zhang, Shaoqing Ren, and Jian Sun. Deep residual learning for image recognition. In *Proceedings of the IEEE conference on computer vision and pattern recognition*, pages 770–778, 2016. 5
- [16] Martin Heusel, Hubert Ramsauer, Thomas Unterthiner, Bernhard Nessler, and Sepp Hochreiter. Gans trained by a two time-scale update rule converge to a local nash equilibrium, 2018. 5, 1
- [17] Jonathan Ho, Ajay Jain, and Pieter Abbeel. Denoising diffusion probabilistic models. In *Advances in neural information processing systems*, pages 6840–6851, 2020. 2
- [18] Jeremy Howard. Imagenet: a subset of 10 classes from imagenet that aren’t so easy to classify, 2019. 5, 1
- [19] Jang-Hyun Kim, Jinuk Kim, Seong Joon Oh, Sangdoon Yun, Hwanjun Song, Joonhyun Jeong, Jung-Woo Ha, and Hyun Oh Song. Dataset condensation via efficient synthetic-data parameterization. In *International Conference on Machine Learning*, pages 11102–11118. PMLR, 2022. 2
- [20] Alex Krizhevsky, Geoffrey Hinton, et al. Learning multiple layers of features from tiny images. 2009. 5
- [21] Saehyung Lee, Sanghyuk Chun, Sangwon Jung, Sangdoon Yun, and Sungroh Yoon. Dataset condensation with contrastive signals. In *International Conference on Machine Learning*, pages 12352–12364. PMLR, 2022. 2
- [22] Tianhong Li, Yonglong Tian, He Li, Mingyang Deng, and Kaiming He. Autoregressive image generation without vector quantization. *Advances in Neural Information Processing Systems*, 37:56424–56445, 2024. 2
- [23] Wenyuan Li, Guang Li, Keisuke Maeda, Takahiro Ogawa, and Miki Haseyama. Hyperbolic dataset distillation. In *The Thirty-ninth Annual Conference on Neural Information Processing Systems*, 2025. 3
- [24] Zongming Li, Tianheng Cheng, Shoufa Chen, Peize Sun, Haocheng Shen, Longjin Ran, Xiaoxin Chen, Wenyu Liu, and Xinggong Wang. Controlar: Controllable image generation with autoregressive models. In *International Conference on Learning Representations*, 2025. 2
- [25] Shilong Liu, Zhaoyang Zeng, Tianhe Ren, Feng Li, Hao Zhang, Jie Yang, Qing Jiang, Chunyuan Li, Jianwei Yang, Hang Su, et al. Grounding dino: Marrying dino with grounded pre-training for open-set object detection. In *European conference on computer vision*, pages 38–55. Springer, 2024. 2
- [26] Yulin Luo, Ruichuan An, Bocheng Zou, Yiming Tang, Jiaming Liu, and Shanghang Zhang. Llm as dataset analyst: Subpopulation structure discovery with large language model. In *European Conference on Computer Vision*, pages 235–252. Springer, 2024. 2
- [27] Zongyang Ma, Guan Luo, Jin Gao, Liang Li, Yuxin Chen, Shaoru Wang, Congxuan Zhang, and Weiming Hu. Open-vocabulary one-stage detection with hierarchical visual-language knowledge distillation. In *Proceedings of the IEEE/CVF conference on computer vision and pattern recognition*, pages 14074–14083, 2022. 2
- [28] Maxime Oquab, Timothée Darcet, Théo Moutakanni, Huy Vo, Marc Szafraniec, Vasil Khalidov, Pierre Fernandez, Daniel Haziza, Francisco Massa, Alaaeldin El-Nouby, et al.

- Dinov2: Learning robust visual features without supervision. *arXiv preprint arXiv:2304.07193*, 2023. 4
- [29] William Peebles and Saining Xie. Scalable diffusion models with transformers. In *Proceedings of the IEEE/CVF international conference on computer vision*, pages 4195–4205, 2023. 1
- [30] Bohao Peng, Zhuotao Tian, Xiaoyang Wu, Chengyao Wang, Shu Liu, Jingyong Su, and Jiaya Jia. Hierarchical dense correlation distillation for few-shot segmentation. In *Proceedings of the IEEE/CVF Conference on Computer Vision and Pattern Recognition (CVPR)*, pages 23641–23651, 2023. 2
- [31] Sucheng Ren, Yaodong Yu, Nataniel Ruiz, Feng Wang, Alan Yuille, and Cihang Xie. M-var: Decoupled scale-wise autoregressive modeling for high-quality image generation. *arXiv preprint arXiv:2411.10433*, 2024. 2
- [32] Olga Russakovsky, Jia Deng, Hao Su, Jonathan Krause, Sanjeev Satheesh, Sean Ma, Zhiheng Huang, Andrej Karpathy, Aditya Khosla, Michael Bernstein, et al. Imagenet large scale visual recognition challenge. *International journal of computer vision*, 115(3):211–252, 2015. 5
- [33] Ahmad Sajedi, Samir Khaki, Lucy Z Liu, Ehsan Amjadian, Yuri A Lawryshyn, and Konstantinos N Plataniotis. Data-to-model distillation: Data-efficient learning framework. In *European Conference on Computer Vision*, pages 438–457. Springer, 2024. 2
- [34] Mark Sandler, Andrew Howard, Menglong Zhu, Andrey Zhmoginov, and Liang-Chieh Chen. Mobilenetv2: Inverted residuals and linear bottlenecks. In *Proceedings of the IEEE conference on computer vision and pattern recognition*, pages 4510–4520, 2018. 5
- [35] Claude E Shannon. A mathematical theory of communication. *The Bell system technical journal*, 27(3):379–423, 1948. 7
- [36] Shitong Shao, Zeyuan Yin, Muxin Zhou, Xindong Zhang, and Zhiqiang Shen. Generalized large-scale data condensation via various backbone and statistical matching. In *Proceedings of the IEEE/CVF Conference on Computer Vision and Pattern Recognition*, pages 16709–16718, 2024. 2
- [37] Jiaming Song, Chenlin Meng, and Stefano Ermon. Denoising diffusion implicit models. In *International Conference on Learning Representations*, 2021. 2
- [38] Duo Su, Junjie Hou, Weizhi Gao, Yingjie Tian, and Bowen Tang. D⁴M: Dataset Distillation via Disentangled Diffusion Model. In *Proceedings of the IEEE/CVF Conference on Computer Vision and Pattern Recognition (CVPR)*, pages 5809–5818, 2024. 2, 3
- [39] Peize Sun, Yi Jiang, Shoufa Chen, Shilong Zhang, Bingyue Peng, Ping Luo, and Zehuan Yuan. Autoregressive model beats diffusion: Llama for scalable image generation. *arXiv preprint arXiv:2406.06525*, 2024. 2
- [40] Peng Sun, Bei Shi, Daiwei Yu, and Tao Lin. On the diversity and realism of distilled dataset: An efficient dataset distillation paradigm. In *Proceedings of the IEEE/CVF Conference on Computer Vision and Pattern Recognition*, pages 9390–9399, 2024. 2, 5, 6
- [41] Mingxing Tan and Quoc Le. Efficientnet: Rethinking model scaling for convolutional neural networks. In *International conference on machine learning*, pages 6105–6114. PMLR, 2019. 5
- [42] Keyu Tian, Yi Jiang, Zehuan Yuan, Bingyue Peng, and Liwei Wang. Visual autoregressive modeling: Scalable image generation via next-scale prediction. In *Advances in neural information processing systems*, 2024. 2, 5, 6
- [43] Saeed Vahidian, Mingyu Wang, Jianyang Gu, Vyacheslav Kungurtsev, Wei Jiang, and Yiran Chen. Group distributionally robust dataset distillation with risk minimization. In *The Thirteenth International Conference on Learning Representations*, 2025. 2
- [44] Aaron Van Den Oord, Oriol Vinyals, et al. Neural discrete representation learning. In *Advances in neural information processing systems*, 2017. 3
- [45] Haoxuan Wang, Zhenghao Zhao, Junyi Wu, Yuzhang Shang, Gaowen Liu, and Yan Yan. Cao2: Rectifying inconsistencies in diffusion-based dataset distillation. In *Proceedings of the IEEE/CVF International Conference on Computer Vision*, pages 4722–4731, 2025. 2, 5
- [46] Kai Wang, Jianyang Gu, Jianyang Gu, Hansong Zhang, Daquan Zhou, Zheng Zhu, Wei Jiang, and Yang You. Dim: Distilling dataset into generative model. In *European Conference on Computer Vision*, pages 42–59. Springer, 2024. 2
- [47] Tongzhou Wang, Jun-Yan Zhu, Antonio Torralba, and Alexei A Efros. Dataset distillation. *arXiv preprint arXiv:1811.10959*, 2018. 2
- [48] Weizhe Yuan, Graham Neubig, and Pengfei Liu. Bartscore: Evaluating generated text as text generation, 2021. 7
- [49] Hao Zhang, Feng Li, Shilong Liu, Lei Zhang, Hang Su, Jun Zhu, Lionel M Ni, and Heung-Yeung Shum. Dino: Detr with improved denoising anchor boxes for end-to-end object detection. *arXiv preprint arXiv:2203.03605*, 2022. 2
- [50] Bo Zhao and Hakan Bilen. Dataset condensation with differentiable siamese augmentation. In *International Conference on Machine Learning*, pages 12674–12685. PMLR, 2021. 2
- [51] Bo Zhao and Hakan Bilen. Dataset condensation with distribution matching. In *Proceedings of the IEEE/CVF Winter Conference on Applications of Computer Vision*, pages 6514–6523, 2023. 2
- [52] Bo Zhao, Konda Reddy Mopuri, and Hakan Bilen. Dataset condensation with gradient matching. *arXiv preprint arXiv:2006.05929*, 2020. 2
- [53] Ganlong Zhao, Guanbin Li, Yipeng Qin, and Yizhou Yu. Improved distribution matching for dataset condensation. In *Proceedings of the IEEE/CVF Conference on Computer Vision and Pattern Recognition*, pages 7856–7865, 2023. 2
- [54] Lin Zhao, Tianchen Zhao, Zinan Lin, Xuefei Ning, Guohao Dai, Huazhong Yang, and Yu Wang. Flasheval: Towards fast and accurate evaluation of text-to-image diffusion generative models. In *Proceedings of the IEEE/CVF Conference on Computer Vision and Pattern Recognition*, pages 16122–16131, 2024. 2
- [55] Lin Zhao, Yushu Wu, Xinru Jiang, Jianyang Gu, Yanzhi Wang, Xiaolin Xu, Pu Zhao, and Xue Lin. Taming diffusion for dataset distillation with high representativeness. *arXiv preprint arXiv:2505.18399*, 2025. 2, 3, 5, 6, 1

- [56] Lin Zhao, Yushu Wu, Aleksei Lebedev, Dishani Lahiri, Meng Dong, Arpit Sahni, Michael Vasilkovsky, Hao Chen, Ju Hu, Aliaksandr Siarohin, et al. S2dit: Sandwich diffusion transformer for mobile streaming video generation. *arXiv preprint arXiv:2601.12719*, 2026. [2](#)
- [57] Xinhao Zhong, Hao Fang, Bin Chen, Xulin Gu, Meikang Qiu, Shuhan Qi, and Shu-Tao Xia. Hierarchical features matter: A deep exploration of progressive parameterization method for dataset distillation. In *Proceedings of the IEEE/CVF Conference on Computer Vision and Pattern Recognition (CVPR)*, pages 30462–30471, 2025. [2](#), [3](#)

HIERAMP: Coarse-to-Fine Autoregressive Amplification for Generative Dataset Distillation

Supplementary Material

A. Algorithm

We provide more details about our coarse-to-fine autoregressive amplify algorithm here. As shown in Algorithm 1, we hierarchically amplify the most salient regions at coarse-to-fine scales, yielding semantics that are maximally informative for classification. We then apply the residual rules described in Sec. 3.1 to obtain the final output. In our final configuration, the amplification factor is set to 5 at all scales and is applied to the weights after the softmax.

B. Generalizing to DiT

To demonstrate that HIERAMP is backbone-agnostic, we extended it to a Diffusion Transformer (DiT) [29] and evaluated it on ImageNet-Woof [18]. Specifically, let A denote the attention output at a given transformer block. We apply spatially guided scaling:

$$\tilde{A} = A \odot (1 + \alpha M), \quad (14)$$

where M is the object-region projected to the token space, α controls the amplification strength, and \odot denotes element-wise multiplication. As shown in Table 5, HIERAMP improves the accuracy while maintaining stable generation compared to the vanilla DiT baseline, which indicates that our method generalizes beyond VAR and is compatible with diffusion-based transformer backbones.

Figure 6 shows visual comparisons before and after applying HIERAMP. We observe enhanced object prominence and clearer semantic structures, while background regions remain largely unaffected or much more relevant. The modulation improves object-level consistency without introducing noticeable artifacts, demonstrating the effectiveness of region-aware scaling in diffusion transformers.

Importantly, this extension requires no architectural re-design and introduces negligible computational overhead. These findings suggest that HIERAMP provides a general mechanism for hierarchical semantic control across diverse generative backbones.

C. FID Comparisons

Comparison with Prior Methods. We compare the Fréchet Inception Distance (FID) [16] of our method with representative dataset distillation approaches, including Minimax [13] and D³HR [55]. FID is computed against the original ImageNet-1K training set under 10 and 50 images per class (IPC). Lower FID indicates better performance.

Algorithm 1 Coarse-to-Fine Semantic Amplification

```

1: Input: Multi-scale queries  $\{Q_n\}_{n=1}^9$ , keys  $\{K_n\}_{n=1}^9$ ,
   values  $\{V_n\}_{n=1}^9$ ; class token is appended as the last
   query in  $Q_n$ , Per-head mask  $\{p_n^{(h)}\}$ ; per-scale key
   counts  $\{L_k^n\}$ ; heads  $H$ , head dim  $d_h$ , Stage schedules
    $(\rho_{1:3}, \rho_{4:6}, \rho_{7:9})$  and  $(\beta_{1:3}, \beta_{4:6}, \beta_{7:9})$ .
2: Output: Amplified attentions  $\{\tilde{\alpha}_n\}$  and/or reweighted
   contexts  $\{\tilde{O}_n\}$ .
3: for  $n = 1$  to 9 do
4:      $\triangleright$  coarse (1–3)  $\rightarrow$  mid (4–6)  $\rightarrow$  fine (7–9)
5:      $(\rho, \beta) \leftarrow \text{STAGEPARAMS}(n)$ 
6:     for  $h = 1$  to  $H$  do
7:          $L_n^{(h)} \leftarrow \frac{Q_n^{(h)}(K_n^{(h)})^\top}{\sqrt{d_h}} + p_n^{(h)}$ 
8:          $\triangleright$  masked logits at scale  $n$ 
9:          $\alpha_{n,\text{cls}}^{(h)} \leftarrow \text{Softmax}(L_n^{(h)}[-1, 1:L_k^n])$ 
10:         $\triangleright$  class  $\rightarrow$  same-scale keys
11:    end for
12:     $m_n \leftarrow \frac{1}{H} \sum_{h=1}^H \alpha_{n,\text{cls}}^{(h)} \in \mathbb{R}^{1 \times L_k^n}$ 
13:     $\triangleright$  head-avg saliency
14:     $k \leftarrow \max(1, \lfloor \rho \cdot L_k^n \rfloor)$ 
15:     $S_n \leftarrow \text{TOPK}(m_n, k)$ 
16:     $a_n \in \{0, 1\}^{L_k^n}$  initialized to 0
17:     $(a_n)_j \leftarrow 1$  iff  $j \in S_n$ 
18:     $\triangleright$  binary indicator
19:    for  $h = 1$  to  $H$  do
20:         $B_n^{(h)} \leftarrow \beta \cdot \mathbf{1}_{L_q^n+1} a_n^\top \in \mathbb{R}^{(L_q^n+1) \times L_k^n}$ 
21:
22:         $\tilde{L}_n^{(h)} \leftarrow L_n^{(h)}$ 
23:         $\tilde{L}_n^{(h)}[:, 1:L_k^n] += B_n^{(h)}$ 
24:         $\tilde{\alpha}_n^{(h)} \leftarrow \text{Softmax}(\tilde{L}_n^{(h)})$ 
25:    end for
26:     $\tilde{O}_n \leftarrow \text{ATTNOUT}(\{\tilde{\alpha}_n^{(h)}\}_{h=1}^H, \{V_n^{(h)}\}_{h=1}^H)$ 
27:
28: end for
29: return  $\{\tilde{O}_n\}_{n=1}^9$ 

```

As shown in Table 6, our method consistently achieves lower FID scores across both IPC settings. In particular, at 10 IPC, our approach improves FID from 18.3 (Minimax) and 19.0 (D³HR) to 17.3. At 50 IPC, we obtain 13.2, outperforming others. We further analyze whether the hierarchical amplification strategy affects generative fidelity. Table 6 reports FID before and after applying HIERAMP on VAR. The results show that FID remains comparable to the

Dataset	Model	IPC	DiT	DiT + HIERAMP
ImageNet-Woof	ResNet-18	10	41.0 ± 0.6	43.1 ± 0.3
		50	66.2 ± 0.3	68.2 ± 0.3

Table 5. **Quantitative comparison of the DiT backbone before and after applying HIERAMP.**



Figure 6. **Qualitative comparison of the DiT backbone before and after applying HIERAMP.**

IPC	Minimax	D ³ HR	VAR	Ours
10	18.3 ± 0.2	19.0 ± 0.2	17.5 ± 0.1	17.3 ± 0.1
50	14.3 ± 0.2	14.9 ± 0.1	13.1 ± 0.1	13.2 ± 0.1

Table 6. **FID of different dataset distillation methods on ImageNet-1K under 10 and 50 IPC.**

default VAR baseline across IPC settings. Specifically, the difference is marginal (e.g., 17.5 vs. 17.3 at 10 IPC).

The above results indicate that HIERAMP preserves visual fidelity while enhancing semantic discriminability. This confirms that the proposed strategy does not degrade generation quality.

D. Effectiveness of Class Tokens

We evaluate the impact of class tokens on both performance and generation quality of VAR. As shown in Tab. 7, models trained with and without class tokens exhibit highly similar top-1 accuracy across different IPC settings, indicating that class tokens introduce no significant advantage or degradation in classification performance.

To further examine their generative behavior, we visualize distilled images produced by both variants in Fig. 7. The “w/o” setting denotes VAR trained without class tokens, while “w/” denotes the standard model with class tokens. Consistent with the quantitative results, the visualizations demonstrate comparable generative capacity: both models produce class-consistent images with similar semantic fidelity and structural detail. These findings show that employing VAR with class tokens is a reliable design choice, and can future provide additional object-focused attention benefits.

E. Computational latency

Comparison with Diffusion Models. We compare the inference speed of our method with a representative diffusion model, DDIM [37] used in D³HR, under the same setting (batch size = 1). As shown in Table 8, our approach

IPC	VAR without class tokens	VAR with class tokens
10	45.9 ± 0.3	45.6 ± 0.3
50	59.5 ± 0.1	59.3 ± 0.1

Table 7. **Effect of class tokens on top-1 accuracy on ImageNet-1K.** Models with and without class tokens show comparable performance across different IPC settings.

Model	Ours	D ³ HR (DDIM-based, 30 steps)
Time (s/img)	0.147 ± 0.001	0.456 ± 0.002

Table 8. **Inference latency comparison with DDIM-based method on ImageNet-Woof.**

Model	Base VAR	VAR + cls	VAR + cls + Amp (Ours)
Latency (s/img)	0.139 ± 0.002	0.145 ± 0.002	0.147 ± 0.001
Peak Memory (GB)	1.770 ± 0.000	1.790 ± 0.000	1.840 ± 0.000

Table 9. **Latency and peak memory for VAR-based distillation with incremental modules.**

achieves significantly lower latency, processing an image in 0.147 s compared to 0.456 s for DDIM with 30 denoising steps. This efficiency arises from the progressive prediction of scales using fewer tokens and a reduced number of inference steps (≤ 10), demonstrating that hierarchical amplification can accelerate generation without sacrificing quality.

Resource Consumption of Distillation. We further report the computational cost of our dataset distillation pipeline based on VAR. Table 9 shows latency and peak memory for the base VAR, VAR with the class token, and VAR with class token plus hierarchical attention amplification (HIERAMP). The additional overhead introduced by the class token and attention modulation is negligible, with runtime increasing only slightly ($0.139 \rightarrow 0.147$ s/img) and peak memory remaining comparable ($1.770 \rightarrow 1.840$ GB).

These results indicate that HIERAMP provides a computationally efficient alternative to standard diffusion-based generation while maintaining competitive fidelity. The progressive scale prediction and token-efficient design contribute to faster inference, and the pipeline ensures minimal runtime and memory overhead for extended VAR variants.

F. Analysis on More Amplification Combinations

We conducted additional experiments with different attention amplification combinations to further validate the conclusions we draw from Fig. 3: (1) amplify Mid & Fine stages by 5 and Coarse stage by 0.5; (2) amplify Coarse & Fine stages by 5 and Mid stage by 0.5; (3) amplify Coarse & Mid stages by 5 and Fine stage by 0.5. As shown in Fig. 3, amplifying attention at coarse and mid scales increases diversity, with many classes exhibiting higher entropy, whereas fine-scale amplification concentrates atten-

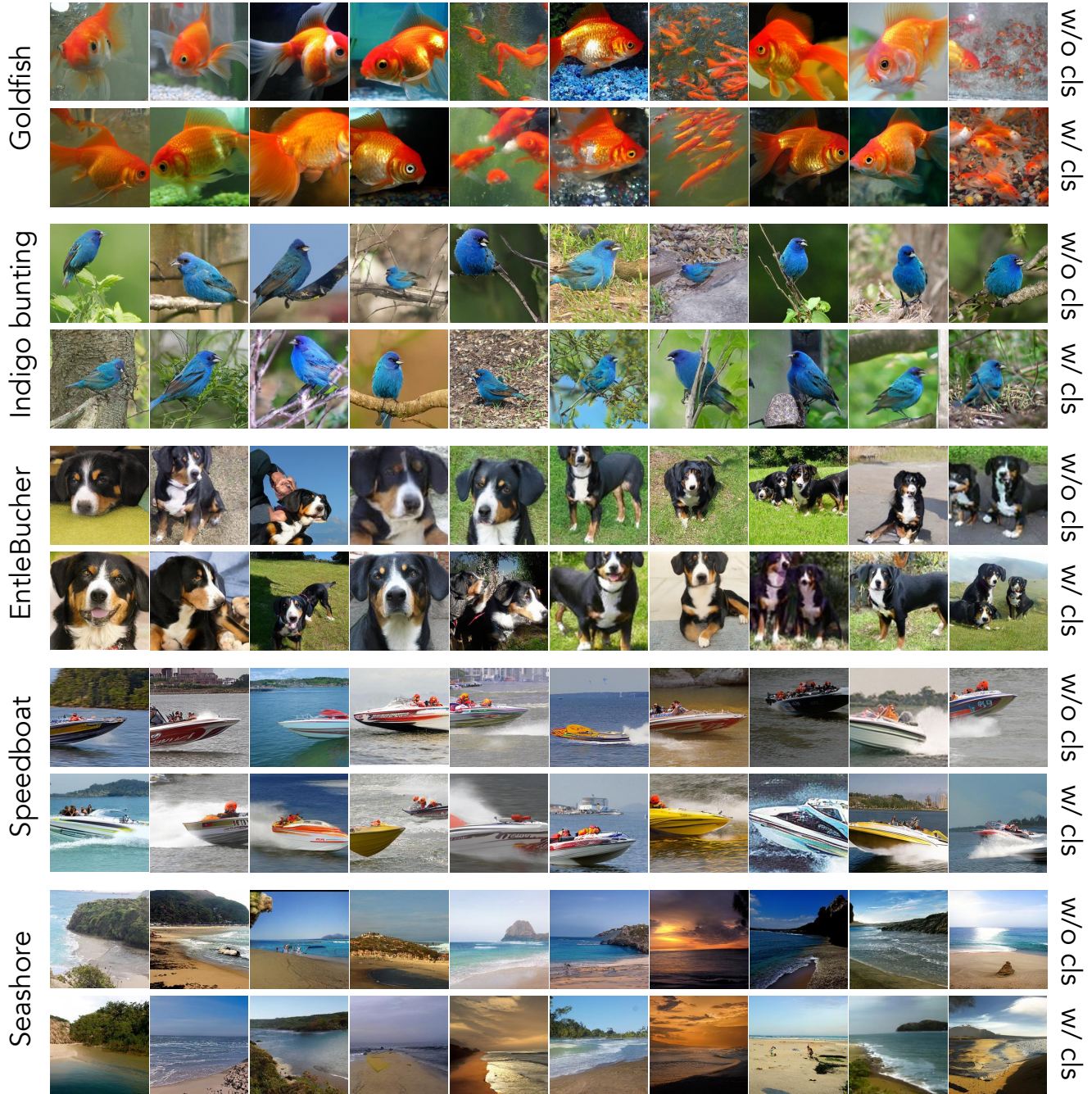


Figure 7. **Visualization of images generated by VAR with and without class tokens on ImageNet-1K, IPC=10.** “w/o” denotes VAR without class tokens, and “w/” denotes VAR with class tokens. The results indicate comparable generative capacity between the two models.

tion, with many classes exhibiting lower entropy.

For combination (1), which is similar to full-stage amplification (S1–S9) except that the Coarse stage is not amplified by 5, but 0.5, we expect fewer classes to exhibit increased token entropy in S1–S3, consistent with the results

in Fig. 8. Similarly, in combination (2), fewer classes show increased token entropy in S4–S6 compared to the full-stage case in Fig. 3. Additionally, reducing the amplification factor in the Fine stage leads to a larger percentage of classes with increased token entropy compared to S7–S9 in Fig. 3,

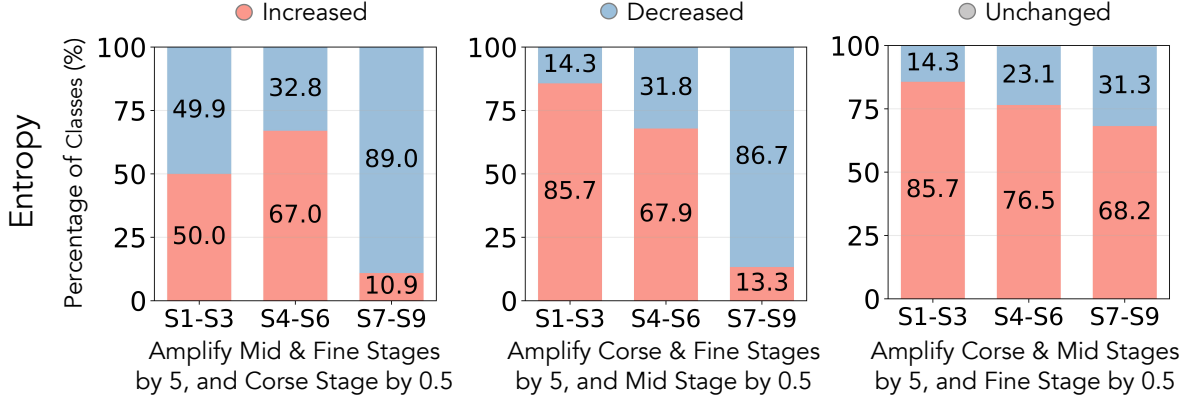


Figure 8. More amplification combinations impact of attention amplification strategy on token entropy on ImageNet-1K, IPC=50.

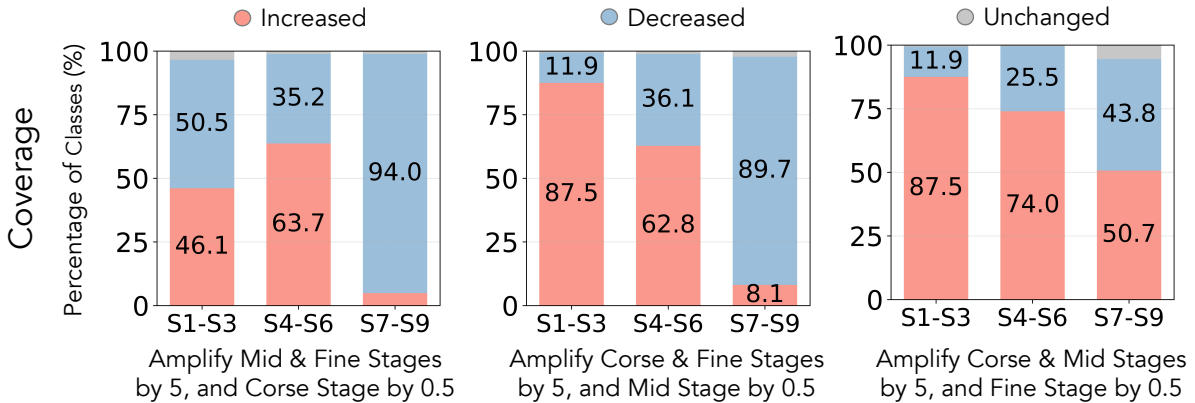


Figure 9. More amplification combinations impact of attention amplification strategy on token coverage on ImageNet-1K, IPC=50.

indicating that smaller amplification at fine scales results in less concentrated attention.

The coverage results in Fig. 9 further corroborate these trends. When amplification is applied to the Coarse and Mid stages, coverage expands across a larger portion of the codebook tokens, reflecting greater diversity in the attended regions. In contrast, stronger amplification at the Fine stage leads to more focused and localized attention, reducing overall coverage. For combination (1), the reduced amplification at the Coarse stage results in lower coverage gains in S1–S3 compared to full-stage amplification. Similarly, combination (2) yields smaller coverage increases in S4–S6, aligning with the patterns observed in the entropy analysis. Finally, combination (3), which applies a weaker amplification to the Fine stage, produces broader coverage in S7–S9 relative to the full-stage setting, consistent with the observation that smaller fine-scale amplification reduces attention concentration.

G. Image Visualization and Comparison

We show further visualizations of the distilled images in this section. As illustrated in Fig. 10 and Fig. 11, HIER-AMP generates finer object detail and more diverse objects in a single image, better semantic alignment, and stronger object–background coupling for each class, providing an effective representation of the full dataset.

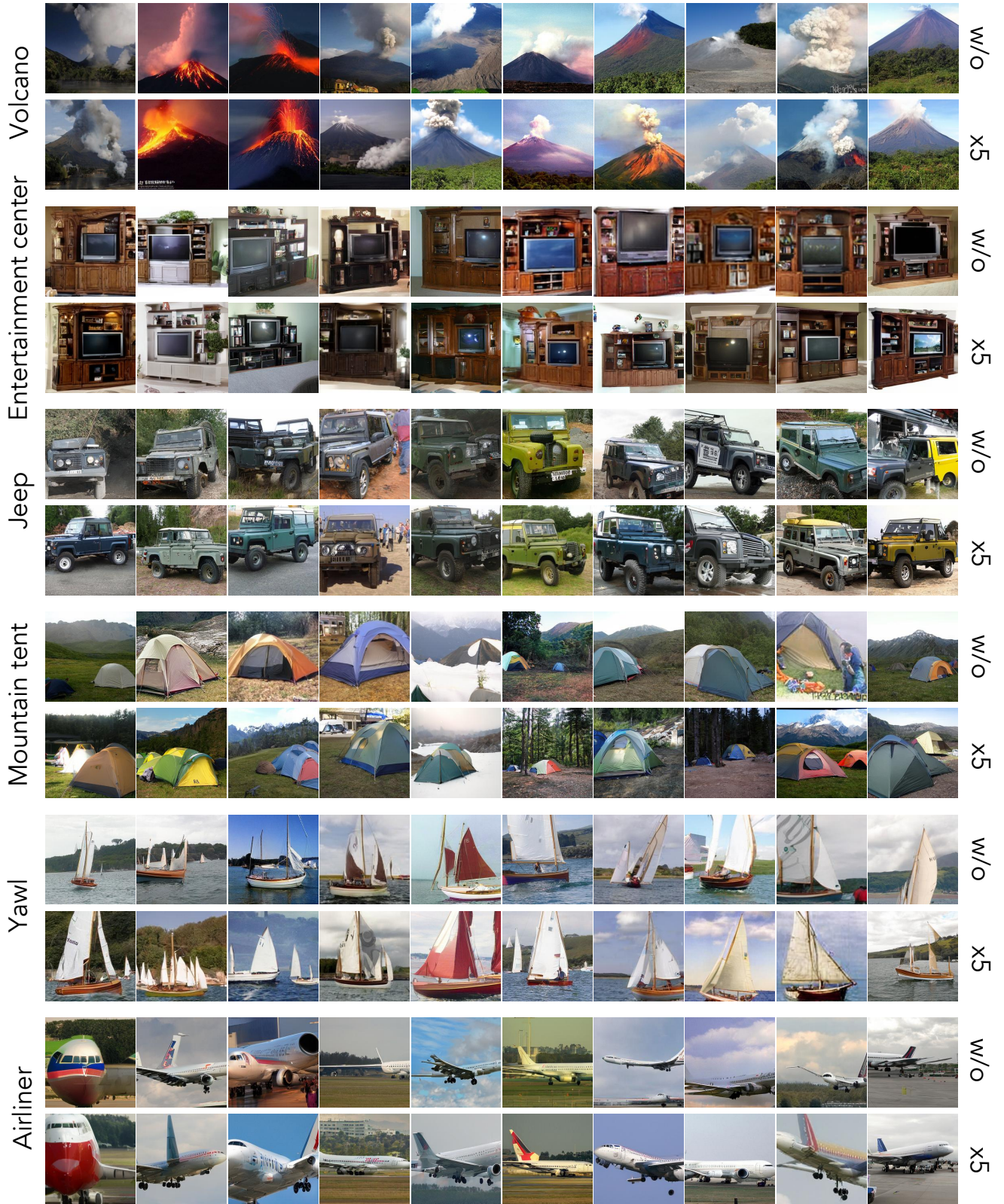


Figure 10. **Visualization of the generated distilled images** (224×224) on ImageNet-1K, IPC=10. The first row shows distilled images without amplification (VAR with class tokens). The second row shows distilled images with amplification applied to Full stages (1-9) by a amplification factor of 5.

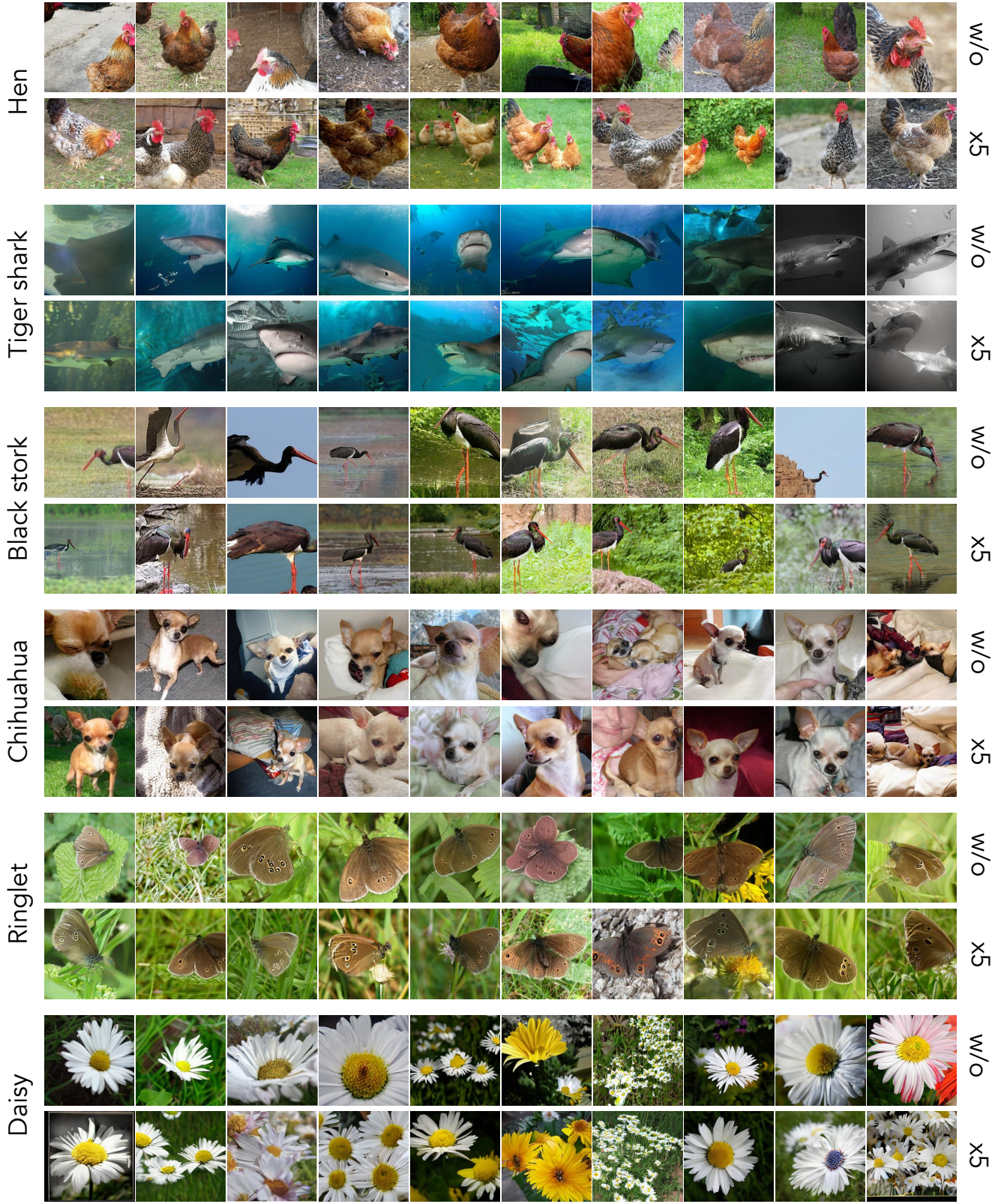


Figure 11. **Visualization of the generated distilled images (224×224) on ImageNet-1K, IPC=10.** The first row shows distilled images without amplification (VAR with class tokens). The second row shows distilled images with amplification applied to Full stages (1-9) by a amplification factor of 5.